Structures under Shock & Impact VI, C.A. Brebbia & N. Jones (Editors)

Modeling shock and projectile penetration response of ceramics

A.M. Rajendran
U.S. Army Research Laboratory
Aberdeen Proving Ground, MD 21005-5069 USA

Abstract

This paper presents the salient features of a spall/microcracking based ceramic damage model and its capabilities in predicting the response of alumina under shock and impact, and projectile penetration. Initially, values for the model parameters were determined using data from planar plate impact (shock) experiments at velocities below and above the Hugoniot elastic limit (HEL). The model's predictive capabilities were examined for penetration of a tungsten rod and a bullet into layered targets.

1 Introduction

There is a strong need for accurate material models in advanced finite element codes that are often used in armor/anti-armor design studies. Since ceramics are important armor materials, several damage models under shock and impact loading conditions were developed during the past decade. The high strain rate and shock response of polycrystalline ceramics is extremely complex and not fully understood. Dynamic deformations in brittle ceramics are due to microcracking, pore collapse, microplasticity, and twinning. There are several models in the open literature that address these various deformation and damage processes.

While some models consider the micromechanics of the damage processes, others use a phenomenological approach to capture the effects of pressure and damage on ceramic compressive strength. The damage process in a brittle ceramic involves nucleation, growth, and coalescence of millions of microcracks (microflaws). The microcracks are of different shapes and sizes. Often, the

Structures under Shock & Impact VI, C.A. Brebbia & N. Jones (Editors)

stress intensity solutions for arbitrary three-dimensional cracks do not exist. The propagation speed of a microcrack under different stress states is extremely difficult to measure and experimental data are not available. The modeling complexity further increases due to the non-linearity and severity of the loading conditions under shock and impact. For practical purposes, the model builders often simplify the constitutive equations through phenomenological descriptions of the salient effects of the deformation and damage processes on the degradation of stiffness and strength of ceramics. In this paper, a model described by Rajendran & Grove [1-3] is briefly presented. The main objective of this paper is to present verification and validation of the material parameters. For this purpose, finite element simulations of projectile penetration into very thick and very thin ceramic tiles were performed.

2 Rajendran–Grove ceramic model

The Rajendran-Grove (RG) ceramic model assumes the following: 1) preexisting randomly distributed flaws, 2) plastic flow when shocked above the Hugoniot elastic limit (HEL), 3) no plastic flow in tension, 4) degradation of elastic moduli under both compression and tension due to microcracking, and 5) pulverization under compressive loading. Above the HEL, the ceramic plastically deforms and the plastic strains are calculated using conventional viscoplastic theories. The elastic strains are then obtained by subtracting the plastic strains from the total strains. The elastic stress-strain equations for the microcracked ceramic material are given by,

$$\sigma_{ij} = M_{ijkl} \left(\varepsilon_{kl} - \varepsilon^{p}_{kl} \right) \tag{1}$$

where σ_{ij} is the total stress, ε_{kl} is the total strain, and ε^{p}_{kl} is the plastic strain due to viscoplastic flow and pore collapse. The components of the stiffness tensor M are given by Rajendran [1]. The elements of this stiffness matrix are degraded through a crack density parameter. The pore collapse strain components were derived from the pressure dependent yield surface of Gurson [4]. Rajendran & Dandekar [5] described the effect of pore collapse on the wave profiles. The strength of the intact ceramic material is described by a strain rate dependent relationship:

$$Y = A \left(1 + C \ln \dot{\varepsilon}^{*} \right) \tag{2}$$

where, A is initial yield strength, C is the strain rate sensitivity parameter, and ε is the normalized equivalent plastic strain rate.

Structures under Shock & Impact VI, C.A. Brebbia & N. Jones (Editors)

In the ceramic model, microcrack damage is defined in terms of a dimensionless microcrack density γ, where $\gamma = N_o^* a^3$. N_o^* is the average number of microflaws per unit volume. The maximum microcrack size, a, is treated as an internal state variable. The microcracks extend when the stress state satisfies a generalized Griffith criterion proposed by Margolin [6]. Microcrack growth causes the crack density γ to increase, which results in stress relaxation in the cracked ceramic material. Since N_o^* is assumed to be a constant, the increase in γ is entirely due to the increase in the crack size a. The damage evolution law is described by,

$$\dot{a} = n_1 C_R \left[1 - \left(\frac{G_{cr}}{G_I} \right)^{n_2} \right] \tag{3}$$

where C_R is the Rayleigh wave speed, G_{cr} is the critical strain energy release rate for microcrack growth, G_I is the applied strain energy release rate, n_1 is the limiting crack growth factor, and n_2 is the crack growth index. In recent applications, the constant n_2 has been assumed a value of one for both tension and compression. G_{cr} is obtained from the fracture toughness K_{IC}, which is a model constant.

Recently, the following spall-parameter-based tensile fracture criterion was speed introduced into the RG model: damage accumulates at the Rayleigh wave when the first principal stress exceeds the spall strength, σ_s, under a tri-axial tensile stress state. The modeling capability was found to substantially improve due to the inclusion of this criterion.

A conventional Mie-Gruneisen equation of state (EOS) is used.

$$P = (\beta_1 \eta + \beta_2 \eta^2 + \beta_3 \eta^3)(1 - 0.5 \Gamma \eta) \tag{4}$$

where η is the volumetric strain and Γ is the Mie-Gruneisen parameter. Table 1 indicates the density (ρ), shear modulus (G), and EOS parameters for 99.5% alumina that were employed in the present investigation.

Table 1. Equation of state and material parameters.

ρ (kg/m^3)	β_1 (GPa)	β_2 (GPa)	β_3 (GPa)	G (GPa)
3890	231	-160	2774	156

The RG model assumes that the ceramic material pulverizes when the γ reaches a critical value of 0.75. The strength Y_p of the pulverized material varies

Structures under Shock & Impact VI, C.A. Brebbia & N. Jones (Editors)

linearly with compressive (positive) pressure P, as $Y_p = \min[Y_{\max}, \beta_p P]$, where β_p is the slope of the strength vs. Pressure plot. Y_{max} is the maximum strength allowed for the confined comminuted ceramic material. An upper limit of 4 GPa was used for AD995, and β_p was assumed to be "1". This simple strength model allows the plastic strains of the pulverized elements (beneath the penetrating projectile) to build up to the critical erosion strain (150%).

3 Model Evaluation

The shock wave profile data measured from plate impact experiments often assist the model parameter determination. In these experiments, a flat thin disk (plate) is made to impact against a target plate. Measurement of the free surface velocity at the rear of the target provides data for the loading (compression) and unloading (release) paths. Plate impact tests are also conducted to measure the Hugoniot Elastic Limit (HEL), which is a measure of compressive strength under one-dimensional strain at very high strain rates. When the release waves interact, tensile stresses of high amplitudes are created in a triaxial stress state subsequently leading to failure of the material.

In the present study, two plate impact experiments were considered: 1) a low velocity (83 m/s) experiment performed by Dandekar & Bartkowski [7] and 2) a high velocity experiment (1943 m/s) reported by Grady & Moody [8]. Dandekar & Bartkowski used a PMMA window behind an 8 mm thick AD995 plate for stress gauge measurements. The AD995 flyer thickness was 4 mm. In the high velocity experiment, a lithium fluoride window backed the AD995 target plate (10 mm). The AD995 flyer thickness was 5 mm. A laser velocity interferometer (VISAR) was used to record the particle velocity history at the target/window interface.

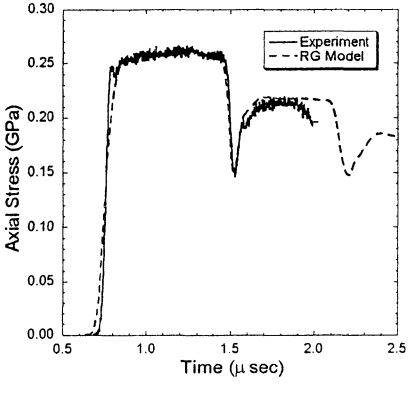

Figure 1. Comparison of EPIC computed stress history with plate impact data for 83 m/s.

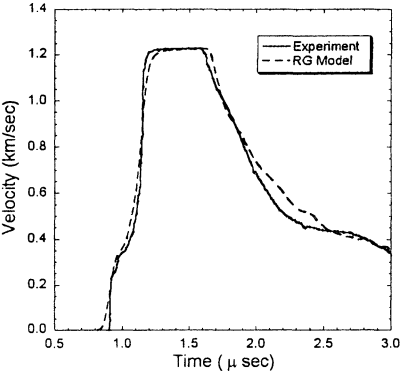

Figure 2. Comparison of EPIC computed velocity history with plate impact data for 1943 m/s.

Structures under Shock & Impact VI, C.A. Brebbia & N. Jones (Editors)

Using a one-dimensional strain option in the EPIC code [9], simulations of the plate impact experiments were performed. The measured spall signal in the 83 m/s test was matched with a value of 0.5 GPa for the critical spall stress σ_s. Fig. 1 shows a comparison between the computed stress history and the experimental data for the 83 m/s plate impact test.

The microcracking model parameters were adjusted until the computed wave profile matched the VISAR data from the high impact velocity test (1943 m/s). In this study, the RG model constants were determined through a series of numerical simulations wherein the values of the initial flaw size (a_o) and the number of flaws per unit volume (N_o^*) were systematically adjusted until the VISAR data (release and spall signals) were matched. A value of 0.1 was assigned to the limiting factor (n_1) for compressive (mode II) crack growth, while n_1 was assumed to be "1" for tensile (mode I) crack growth. The calibrated RG model constants are: K_{IC} = 3 MPa$\sqrt{\text{m}}$, n_1 = 0.1 (mode II crack growth), a_o= 1 μm, N_o^* = 2x10^{11} m^{-3}, and μ = 0.45, where μ is the dynamic coefficient of friction that appears in the Griffith criterion. Simulations also revealed that when the tri-axial stress based spall criterion was not included in the microcracking model, unrealistic large values for the initial microcracks had to be assumed in order to match the low velocity spall data. With the spall criterion, realistic values for the microcracks (< 5 microns) comparable to average grain sizes were used in the modeling of AD995.
Using these constants, the velocity vs. time signal from the 1943 m/s test was successfully matched as shown in fig. 2. In the simulation, the strain rate sensitivity parameter B seems to influence the slope of the release portion of the VISAR signal. A value of 0.2 that is consistent with the strain rate dependency of AD995 reproduced the release portion very well. In general, the RG model reproduced the one-dimensional shock data extremely well.

Rajendran and Grove [3] presented results from modeling the depth of penetration (DOP) experiments of Woolsey [10] in which a tungsten long rod projectile was launched at a velocity of 1.5 km/s onto a ***thick*** 152 mm square ceramic tile that is laterally confined by a steel frame as well as a thick steel backup block. The ceramic tiles were 25, 38, and 50 mm thick. Using the 2D axi-symmetric option in EPIC, the DOP configurations were modeled. The plate impact matched RG model constants for AD995 were employed in this simulation. The model prediction agreed with the measured DOP within 10 percent.

To further validate the model constants, a two-layer target with a ***thin*** *(5mm)* ceramic tile was considered. The target in this study was a 150 mm x 150 mm x 5 mm ceramic tile bonded to a 100 mm thick aluminum plate. The projectile (shown in Fig. 3) was a 30-caliber, armor-piercing projectile (APM2). The striker velocity was 890 m/s.

Structures under Shock & Impact VI, C.A. Brebbia & N. Jones (Editors)

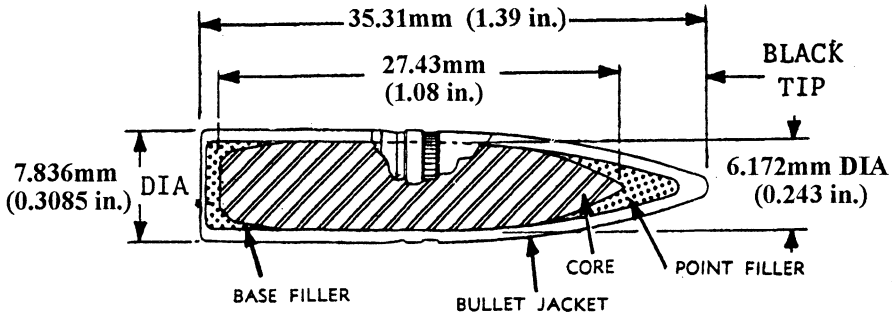

Figure 3. A schematic of 30 Caliber Armor-Piercing Projectile.

The bullet's jacket is made of a gilding (copper base) metal with a mass of 4.21 gm. The hardened alloy steel core weighs 5.25 gm. The weight of the lead filler is 0.5 gm. The total weight of the APM2 is 10.74 gm. In the ballistic tests, the projectiles penetrated through the ceramic tiles and stopped inside the aluminum backing plates. The depth that the projectile penetrated into the backing plate is called the residual depth of penetration that is measured by using x-ray radiograph.

The ballistic experiments were numerically simulated using the two-dimensional axisymmetric geometry option in the EPIC code. The EPIC library constants were used in the material descriptions for the lead, copper, and steel. In the simulations, the calibrated RG model constants were employed to describe the thin (5 mm) AD995 ceramic tile. In ballistic tests, the projectile's hardened steel core has been observed to fracture in a brittle manner. In the simulations, the projectile elements were assumed to fail based on the Johnson-Cook fracture criterion and to erode at a critical strain value of 1.5.

In the simulation, the ceramic began to damage directly beneath the projectile. Within the first 5 microseconds, a conical fracture zone evolved in the ceramic. Further on in the simulation, Herzian type cracks (ring shaped) appeared on the top surface of the ceramic at about two projectile radii and penetrated into the ceramic at an angle. These damage fronts turned horizontal and extended rapidly along the radial direction. The spread of the damage qualitatively agreed with the posttest observations as can be seen from Figures 4a and 4b.

The projectile completed its penetration of the ceramic tile after about 40 microseconds. It continued penetrating into the aluminum plate and finally stopped inside the aluminum. The simulations accurately predicted the final depth of penetration into the aluminum. In general, results from the simulations of plate impact and ballistic experiments using the microcrack-based RG ceramic damage model agreed reasonably well with the experimental data.

Structures under Shock & Impact VI, C.A. Brebbia & N. Jones (Editors)

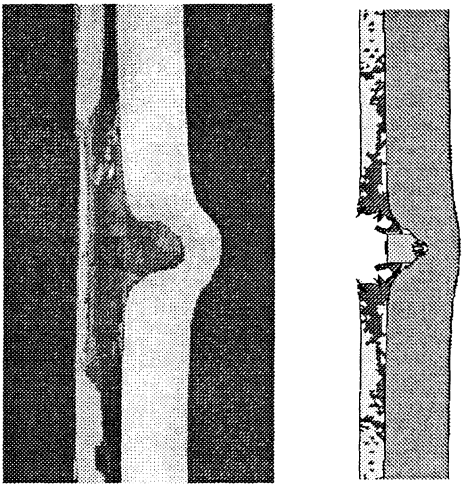

(a) (b)

Figure 4. The final cross section of the two-layered (ceramic/aluminum) target: (a) test result; (b) simulation.

4. Summary

The shock and impact response of AD995 ceramic was modeled using a spall/microcracking based ceramic damage model. The model constants were initially calibrated by matching the simulated stress history with the stress gauge data from a low velocity plate impact test at 83 m/s and the velocity history with the VISAR data from a high velocity test at 1943 m/s. The critical stress (σ_s) based spall criterion was used to model the spall signal in the low velocity experiment. The microcracking model constants were calibrated to reproduce the high velocity experimental data. The strength constants $Y_{\max}$ *and* β_p for the pulverized ceramic were adjusted to reproduce the depth of penetration (DOP) of a tungsten rod into a 25 mm thick ceramic plate; this did not require any further adjustments to the RG model constants determined from the plate impact experimental data. Two other DOP data for 38 and 50 mm thick ceramic tiles were successfully predicted. As a final verification, an APM2 penetration into a layered thin target plate was successfully predicted using the calibrated model constants. The results from the finite element simulations qualitatively compared the observed damage evolution in the posttest targets from ballistic experiments. he present study showed how the RG model parameters could be determined from a variety of shock and penetration experiments. The last application further validated the RG model's capabilities in capturing several salient features of the ceramic damage under shock and impact.

References

[1] Rajendran, A.M., Modeling the Impact Behavior of AD85 Ceramic Under Multiaxial Loading, *Int. J. Impact Engng.*, 15 (6) pp. 749-768, 1994.

[2] Rajendran, A.M. & Grove, D.J., Modeling the Shock Response of Silicon Carbide, Boron Carbide, and Titanium Diboride, *Int. J. Impact Engng.*, 18 (6) pp. 611-631, 1996.

[3] Rajendran, A.M. & Grove, D.J., Modeling of Shock and Impact Behaviors of Aluminum Oxide. *Structures Under Shock and Impact V* – Eds., N. Jones, D.G. Talaslidis, C.A. Brebbia, and G.D. Manolis. Computational Mechanics Publications, pp. 447-460, 1998.

[4] Gurson, A.L., Continuum Theory of Ductile Rupture by Void Nucleation and Growth; Part I: Yield Criterion and Flow Rules for Porous Ductile Materials. *J. Engr. Mat. Tech.*, 99, pp. 2-15, 1977.

[5] Rajendran, A.M. & Dandekar, D.P. Inelastic Response of Alumina. *Int. J. Impact Engng.*, 17, pp. 649-659, 1995.

[6] Margolin, L.G. A generalized Griffith Criterion for Crack Propagation. *Engineering Fracture Mechanics,19, pp. 539-543, 1984.*

[7] Dandekar, D.P. & Bartkowski, P., Shock Response of AD995 Alumina, *High-Pressure Science and Technology - 1993, Part 2,* AIP Press, pp. 733-736, 1994.

[8] Grady, D.E. & Moody, R.L., *Shock Compression Profiles in Ceramics*, Sandia Report, SAND96-0551, March 1996.

[9] Johnson, G.R., Stryk, R.A., Petersen, E.H., Holmquist, T.J., Schonhardt, J.A., & Burns, C.R., *User Instructions for the 1995 Version of the EPIC Code*, Alliant Techsystems Inc., Brooklyn Park, Minnesota, November, 1994.

[10] Woolsey, P., unpublished work at AMTL, Watertown, MA, 1991.